ELSEVIER

Tectonophysics 326 (2000) 111–130

TECTONOPHYSICS

www.elsevier.com/locate/tecto

# Strain partitioning in the northern Walker Lane, western Nevada and northeastern California

Patricia H. Cashman *, Sheryl A. Fontaine

*Department of of Geological Sciences, University of Nevada, Reno NV 89557, USA*

**Abstract**

Paleomagnetic studies constrain both the kinematics and the timing of Neogene intracontinental strain in the Walker Lane of northwestern Nevada–northeastern California. The northwest-trending Walker Lane is a zone of complex faulting and dextral offset along the boundary between the Sierra Nevada and the Basin and Range. Here, an extensive Tertiary volcanic section provides a paleomagnetic test for vertical-axis rotation. The 25.1 Ma Nine Hill tuff covered the two structural domains of northern Walker Lane and parts of the adjacent provinces. In the northernmost domain, the Pyramid Lake domain, the Nine Hill tuff is unrotated or rotated slightly counter-clockwise. In contrast, Nine Hill tuff is rotated 35–44° clockwise in the northeastern part of the adjacent Carson domain. Usable exposures of the tuff are lacking elsewhere in the Carson domain, but 9–13 Ma basalts record 37°–51° clockwise vertical-axis rotation. These basalts were sampled at three sites encompassing the N–S length of the Carson domain. Younger basalts from the Carson domain show smaller clockwise rotations. The paleomagnetic studies show that the deformation in the northern Walker Lane is partitioned into domains dominated by translation, rotation and extension. Dextral slip along the Walker Lane is accommodated primarily by northwestward translation in the Pyramid Lake domain, and by clockwise vertical-axis rotation in the Carson domain. Some Neogene extension is also accommodated in the Walker Lane, but most of it is occurring to the west of the Walker Lane, along the edge of the Sierra Nevada.Comparison of paleomagnetic results from rocks of different ages constrains the timing of the present deformation regime in the Walker Lane. The similar rotations recorded in 25 Ma and 9–13 Ma rocks indicates that virtually all of the rotation in the Carson domain occurred after the eruption of the 9–13 Ma basalts. Smaller rotations recorded in younger rocks constrain rotation rate. 

*Keywords:* Walker Lane; strain partitioning; block rotation; intracontinental strain

## 1. Introduction

In the western USA, active crustal deformation is distributed across the western third of the continent, well away from the North America–Pacific plate boundary. At present, the intraplate strain in the Basin and Range is broadly partitioned, with extension in most of the province and a zone of dextral slip (the Walker Lane and Eastern California Shear Zone) along the western margin. The dextral slip zone is thought to accommodate much of the relative plate motion that is not taken up along the San Andreas system, the present plate boundary (e.g. Atwater, 1970; Zoback et al., 1981; Dokka and Travis, 1990). Both the extension and the dextral slip are exceptions to the general rule that lithospheric plates are rigid, with deformation confined to the immediate vicinity of the plate margins. Long-standing debates about the style

* Corresponding author.

0040-1951/00/$ - see front matter 
PII: S0040-1951(00)00149-9

and timing of Basin and Range deformation, as well as more recent ones about the westward encroachment of extension into the eastern Sierra Nevada or the kinematics and timing of deformation in the Walker Lane or Eastern California Shear Zone, pertain to more fundamental issues — the tectonic factors that influence this crustal-scale, intra-plate deformation.

The Walker Lane was originally identified as the physiographic zone marking the western edge of the north-northeast-trending, fault-bounded mountains of the Basin and Range province (Locke et al., 1940). It is a zone of complex faulting and dextral shear. As initially described, it extends from Honey Lake, California in the north to the latitude of Las Vegas, Nevada in the south, and lies along the boundary between the Basin and Range and the Sierra Nevada (Fig. 1). Recent mapping indicates that the zone of faulting and dextral shear continues still farther to the northwest (e.g. Grose et al., 1989; Grose, 1993, and references therein).

Stewart (1988) divided the Walker Lane into nine structural domains, based on the orientation

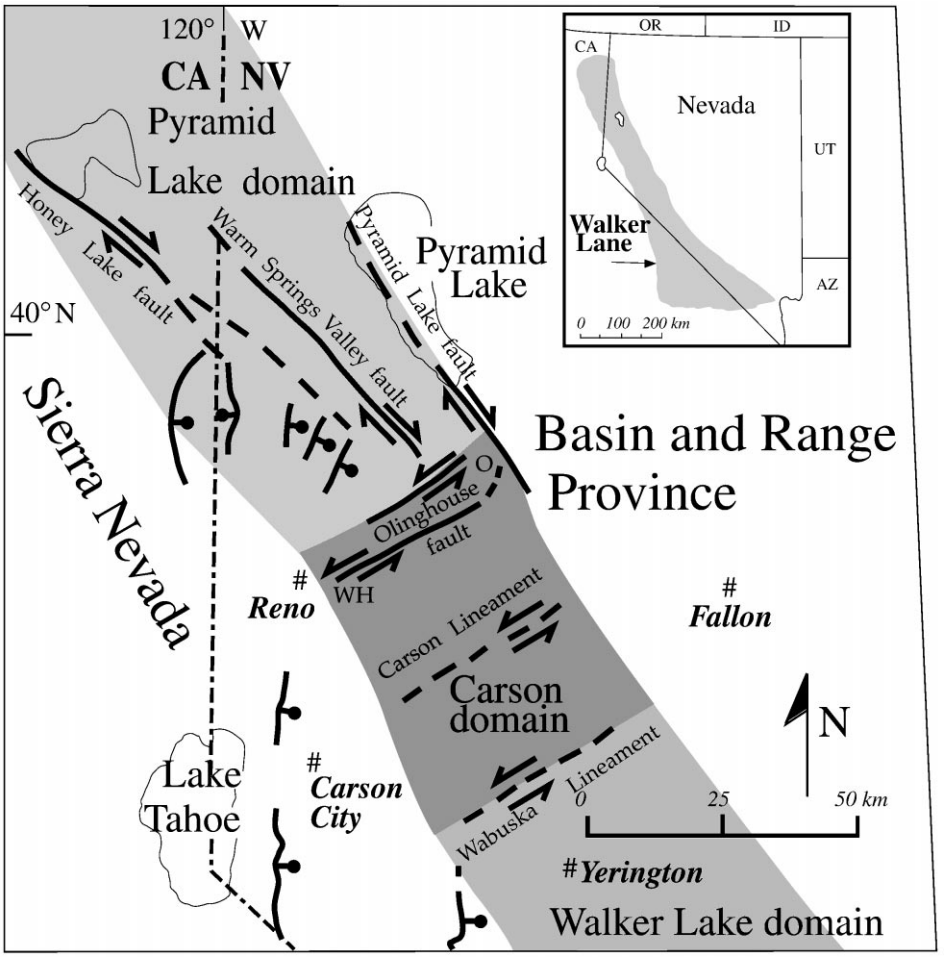


Fig. 1. Location map of the northern Walker Lane, showing the three northern structural domains of Stewart (1988) and the names of the major strike–slip faults in the Pyramid Lake domain and the Carson domain. Sense of motion shown for strike–slip faults: down-dropped block shown by ball and bar symbol for normal faults. O, Olinghouse mining district; WH, Washington Hill mining district.

of map-scale faults (Fig. 1). The northern three, from north to south, are the Pyramid Lake domain, the Carson domain and the Walker Lake domain. The Pyramid Lake and Walker Lake domains are characterized by northwest-trending dextral faults. The Carson domain is characterized by east-northeast-trending lineaments and sinistral faults. Although tens of kilometers of dextral offset along northwest-trending faults has been demonstrated in the Pyramid Lake and Walker Lake domains (see below), the intervening Carson domain has no known through-going northwest-trending faults.

The goal of this research was to determine the mechanism for transmitting significant northwest-directed dextral slip across the Carson domain, where there are no major northwest-striking faults. Our approach has been to combine structural studies, which document the orientation and kinematics of faulting, with paleomagnetic studies on Tertiary volcanic rocks, which measure vertical-axis rotation. We chose the 25.1 Ma Nine Hill tuff for paleomagnetic studies, because of its wide distribution across the northern Walker Lane and adjacent Sierra Nevada (inset map in Fig. 2), and because its age and paleomagnetic reference direction are well established (Deino, 1985; 1989). Usable exposures of Nine Hill tuff are inadequate to characterize vertical-axis rotation throughout the Carson domain, so our paleomagnetic studies there include late Miocene and Pliocene basalts.

In this paper, we present the results of paleomagnetic studies in the Pyramid Lake and Carson structural domains of the northern Walker Lane. We review the regional geologic setting to provide the context for the choice of geologic units and sampling localities for paleomagnetic analysis. We then summarize our paleomagnetic data, grouped first by structural domain and then (within the Carson domain) by decreasing age of the volcanic rocks studied. We present a kinematic model consistent with both the paleomagnetic results and the map-scale structures. We conclude with our new understanding of the style and timing of deformation in the northern Walker Lane. The timing of inception of the present regime of dextral slip constrains tectonic models for Walker lane deformation.

## 2. Geologic setting

The Sierra Nevada-Basin and Range transition zone contains extensive and well-exposed Neogene stratigraphic sections, including both igneous and sedimentary rocks. The region has undergone nearly continuous volcanism from the Oligocene to the Quaternary (Silberman et al., 1979; Deino, 1985; Garside and Bonham, 1992; Saucedo and Wagner, 1992; Stewart et al., 1994), encompassing a compositional range from basalts to rhyolites. During the late Oligocene and earliest Miocene, ash-flow tuffs blanketed much of the region. Recent $^{40}Ar/^{39}Ar$ dates indicate two pulses of ash-flow tuff eruption, one ca. 30 Ma and one at 25 Ma (Deino, 1989; dates by C.D. Henry, reported in Garside and Niles, 1998; Castor et al., 1999; Garside et al., 1999; John et al., 1999). The 25.1 Ma Nine Hill tuff, chosen for paleomagnetic analysis in this study, is the most widespread of these tuffs (Deino, 1985) (Fig. 2). Since ca. 20 Ma, volcanism has been primarily effusive. Rock types are dominantly dacitic to andesitic lavas, but range from basalt to rhyolite lava domes. In general, these rocks record the presence of a volcanic arc. Basalt and basaltic andesites used in this study are from two map units — the older Pyramid sequence basalts (9–13 Ma), and the younger Lousetown basalts (5–7 Ma). Unit designations for the localities studied are from Bonham (1969). Ages for these localities are from Stewart et al. (1994).

The Pyramid Lake and Carson domains each contain several major, en echelon strike–slip faults which are reflected in the topography (Fig. 1). The intervening fault-bounded blocks are locally faulted (e.g. Fontaine, 1997), but these faults appear to be confined to the blocks rather than being through-going structures. There are three major left-stepping dextral faults in the Pyramid Lake domain; from north to south, these are the Honey Lake fault, Warm Springs Valley fault and Pyramid Lake fault. The sinistral Olinghouse fault system forms the northern boundary of the Carson domain, and the Wabuska lineament forms its southern boundary. There is a mapped fault along part of this boundary (Moore, 1969; Greene et al., 1991), but the feature as a whole is generally described as a topographic lineament rather than

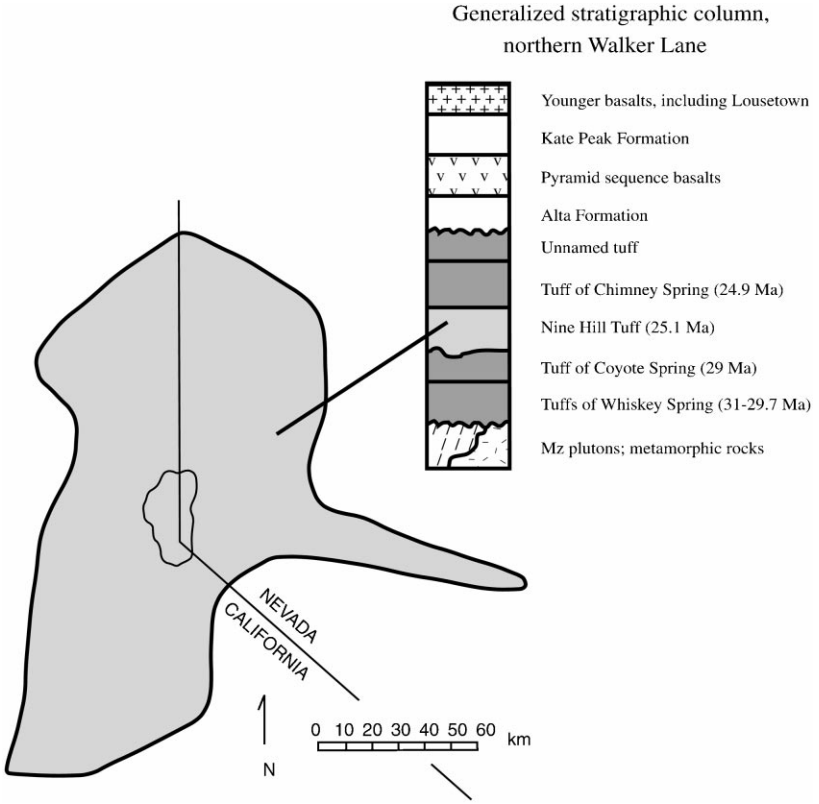


Fig. 2. Generalized stratigraphic column for the northern Walker Lane, modified from Garside and Bonham (1992). The three stratigraphic units used in this study are the Nine Hill tuff and basalts from the Pyramid sequence and the Lousetown basalt. Age of Nine Hill tuff from Deino (1989); ages of other tuffs from dates by C.D. Henry, reported in Garside and Niles (1998); Castor et al. (1999); Garside et al. (1999); John et al. (1999). See text for basalt ages at each sample locality. Map, from Deino (1985), shows geographic distribution of the Nine Hill tuff.

as a through-going fault. Similarly, the Carson lineament, in the central part of the domain, has numerous Pleistocene and some Holocene fault scarps (Bell, 1984), but bedrock contacts are generally covered by alluvium, and the feature is not generally mapped as a through-going fault.

The central Walker Lane, which extends south from the Carson domain, is one of the most extensively studied parts of the Walker Lane; total offset and timing of dextral, 'Walker Lane-style' deformation are best known here. The total dextral offset across the central Walker Lane is a minimum of 48–60 km (Ekren and Byers, 1984; Ekren, 1985a,b, 1986a,b; Hardyman et al., 1975; Hardyman and Oldow, 1991; Oldow, 1992; Speed and Cogbill, 1979). This offset has occurred in the last 27 Ma, during several distinct faulting episodes (Hardyman, 1984; Ekren and Byers, 1984; Hardyman and Oldow, 1991; Oldow, 1992; Dilles and Gans, 1995). Although there is some disagreement about the timing and kinematics of these faulting episodes, most workers agree that normal and strike–slip faulting occurred, maybe as several distinct events, between 22 and 27 Ma. The extreme extensional faulting at Yerington occurred between 12.5 and 14 Ma (Dilles and Gans, 1995). The present dextral strike–slip faulting began as recently as 7 Ma (Dilles and Gans, 1995) to 10 Ma (Hardyman and Oldow, 1991).

The northern Walker Lane has been mapped at a regional scale (e.g. Bonham, 1969; Moore, 1969; Greene et al., 1991; Stewart, 1999; and many

others), but studies of fault kinematics, volcanic stratigraphy and geochronology are available only locally. The style and timing of faulting is not as well understood as it is in the central Walker Lane. Cumulative offset is not well documented and may decrease northward. Bonham (1969, and personal communication, 1993) estimates 30–40 km of dextral offset in Washoe Co., Nevada, based on offset of the Tertiary/pre-Tertiary contact. In northeastern California, Grose (1993) estimates not more than 20 km of dextral offset since mid-Miocene time. Timing information in the northern Walker Lane is also limited. In the Pyramid Lake domain, some northwest-striking faults existed prior to mineralization dated at $21.8 \pm 0.7$ Ma (Stewart et al., 1994). Elsewhere in the domain, a northwest-striking fault offsets a $20.82 \pm 0.1$ Ma dike 2.3 km in a dextral sense, but this fault shows no evidence of Holocene activity (Garside and Niles, 1998). Parts of all three major northwest-striking dextral faults have moved in Holocene time (e.g. Wills and Borchardt, 1993; Anderson and Hawkins, 1984; Bell, 1984). In the Carson domain, northeast-striking faults in the Olinghouse district, at the east end of the Olinghouse fault system, existed prior to mineralization dated at $10.46 \pm 0.03$ Ma (John et al., 1999). At the west end of the Olinghouse fault system, 12.9–10 Ma mineralization in the Washington Hill district (Vikre et al., 1988) has been offset $>2$ km along a northeast-striking sinistral fault (Albino, 1992). Different parts of the Olinghouse fault have moved in Pleistocene, Holocene and historic time (Bell, 1984).

## 3. Methodology and data characteristics

This paper presents newly acquired paleomagnetic data for 17 sites collected from the 25.1 Ma Nine Hill tuff (123 samples used, of 183 analyzed) and 57 sites collected from five localities in younger basalts (360 samples used, of 450 analyzed). An additional 12 tuff sites and two basalt localities (20 flows) were sampled and analyzed, but results were not used because of: (1) secondary magnetic overprints or anomalous inclinations, discussed below, which preclude interpretation of vertical-axis rotations (for Nine Hill tuff sites); or (2) unstable magnetic mineralogy or anomalous transient paleofield orientations (for basalt sites). The results for the omitted Nine Hill tuff sites are indicated with superscript "b" in Table 1. Samples were collected with a portable rock drill, and were oriented with a clinometer and both solar and magnetic compasses. At most sites, 6–12 samples were collected from outcrops in an area of several square meters to tens of square meters. The orientation of compaction foliation in the Nine Hill tuff was determined from the abundant flattened pumice fragments. Orientations of lava flows were derived from three-point calculations over relatively large areas, using aerial photographs and a PG-2 plotter. Tilt corrections were made by rotating about the strike. Dips of bedding were generally low ($<10^\circ$ for all but one of the basalt sites, and $<35^\circ$ for all but six of the Nine Hill tuff sites) (Table 1), so the error induced by rotating about the strike line is minimal for most samples. It is worth noting here, however, that there is considerable paleotopography at the basal contact of the Nine Hill tuff. Locally, compaction foliation measured in the tuff mimics this topography, and does not record paleohorizontal. In some cases, mapping in the immediate vicinity of the sampling site could resolve this problem, but in others, an incorrect tilt correction may be the reason for an anomalous inclination and, therefore, unusable results.

In the laboratory, samples were treated by progressive thermal and alternating field demagnetization. Pilot studies showed that the best demagnetization sequence for the Nine Hill tuff was three thermal demagnetization steps (100–200°C) followed by five alternating field steps with peak inductions of 60 millitesla (mT) (Fontaine, 1997). A similar sequence was used for most of the basalt samples, usually with fewer thermal and more alternating field steps, and peak inductions of 60 to 80 mT. Demagnetization results were plotted on vector diagrams (Fig. 3). The orientation of the remanent magnetism was determined using a least-squares fit on visually identified, linear segments of the demagnetization path (Kirschvink, 1980). Site means were determined from the averages of sample directions, giving unit weight to each sample. Dispersion parameters (Table 1)

Table 1
Paleomagnetic data [a]

| Site | Lat. °W | Long.°N | $N/N_o$ | $\kappa$ | $\alpha_{95}$ | *Dg* | *Ig* | *St/Dp* | *Ds* | *Is* | Locality | Rotation |
|---|---|---|---|---|---|---|---|---|---|---|---|---|
| *Nine Hill Tuff* | | | | | | | | | | | | |
| NHCA | 39.21 | 119.73 | 4/10 | 96.8 | 9.4 | 11 | 60.7 | 199/28 | 334.8 | 47.7 | Carson Arprt | −0.2±12.1 |
| NHFS | 40.01 | 119.94 | 8/10 | 884.9 | 1.9 | 344 | 46 | 094/26 | 322.1 | 69.1 | Fort Sage | −12.9±6.2 |
| NHHR01 | 39.75 | 119.70 | 6/10 | | 5.8 | 21.5 | 55.7 | 032/39 | 75.2 | 49.2 | Hungry Ridge | 100.2±8.4 |
| NHLV01 | 39.67 | 119.78 | 6/10 | 935.4 | 1.7 | 82.9 | 31.2 | 172/84 | 258.1 | 64.2 | Lemmon Valley | −76.9±5.5 |
| NHLV02 | 39.68 | 119.77 | 5/10 | 272.6 | 4.6 | 195.5 | 84.2 | 245/32 | 326.4 | 62.2 | Lemmon Valley | −8.4±9.1 |
| NHMC | 39.9 | 119.69 | 36350 | 344.2 | 2.2 | 312.9 | 54.3 | 006/30 | 8.6 | 69.2 | Mine Canyon | 33.6±6.7 |
| NHMP | 39.90 | 119.68 | 6/10 | 449.3 | 3.2 | 315.2 | 48.2 | 013/15 | 322.2 | 62.4 | Maue Point | −12.8±7.2 |
| NHMS | 39.94 | 119.82 | 8/10 | 247.1 | 3.5 | 279.1 | 61.2 | 272/18 | 311.1 | 59.4 | McKissick Spg | −23.9±7.1 |
| NHPA | 39.77 | 119.65 | 8/8 | 214.0 | 3.8 | 41 | 70.5 | 185/32 | 329.7 | 58.8 | Pah Rah Range | −5.3±7.4 |
| NHPM | 39.90 | 119.94 | 6/12 | 392.7 | 3.4 | 344.3 | 24 | 065/46 | 331.9 | 69 | Porcupine Mtn | −3.1±8.9 |
| NHPR01 | 39.53 | 119.28 | 36446 | 306.6 | 2.8 | 49.9 | 67.7 | 236/22 | 10.2 | 57.6 | Painted Rock | 35.2±6.2 |
| NHPR02 | 39.60 | 119.36 | 36477 | 99.8 | 4.0 | 59.8 | 59.1 | 229/31 | 19.1 | 47.8 | Painted Rock | 44.1±6.6 |
| NHRC | 39.77 | 119.56 | 36291 | 137.8 | 5.7 | 37.3 | 26.6 | 133/25 | 34.8 | 51.4 | Right−hand Can | 59.8±8.6 |
| NHRR | 39.90 | 120.00 | 8/14 | 88.2 | 6.5 | 69.6 | 75.2 | 186/42 | 317.5 | 57.7 | Red Rock | −17.5±10.8 |
| NHSC | 39.20 | 119.66 | 36350 | 211.1 | 4.9 | 334.9 | 65.3 | 199/21 | 315.6 | 48.3 | Santiago Can | −19.5±15.1 |
| NHSL | 39.92 | 119.92 | 8/10 | 628.1 | 2.1 | 266.2 | 64.2 | 311/46 | 5 | 57.6 | Seven Lakes | 30.0±5.5 |
| NHTC | 39.89 | 119.87 | 8/9 | 333.4 | 3.0 | 26.3 | 16.3 | 137/41 | 13.1 | 53 | Tick Canyon | 38.1±6 |
| NHBF[b] | 39.76 | 119.68 | 8/ | 464.9 | 2.2 | 53.1 | 60.9 | 248/36 | 15.4 | 39.1 | Bacon Rind Flat | 40.4±5.1 |
| NHCR[b] | 39.18 | 119.69 | 36381 | 164.5 | 4.0 | 320.3 | 66.1 | 286/47 | 353.6 | 27.1 | Carson River | 24.0±11 |
| NHCRE[b] | 39.79 | 119.58 | 36169 | | | 325.2 | 67.8 | 151/34 | 277.3 | 47.7 | Chukar Ridge | −79.6 |
| NHDV[b] | 39.95 | 119.93 | 36411 | 41.9 | 8.1 | 13.2 | 35.4 | 266/58 | 10.9 | −20.6 | Dry Valley | 35.9±8.3 |
| NHEC[b] | 39.22 | 119.71 | 36354 | 6.2 | 26.4 | 103.9 | 42.4 | 143/24 | 128.2 | 53.3 | East Carson | 153.2±38 |
| NHHR02[b] | 39.75 | 119.7 | 36284 | 1.8 | 59.3 | 82.8 | −11.8 | 032/39 | 69.1 | −33.5 | Hungry Ridge | 94.1±25.8 |
| NHHR03[b] | 39.73 | 119.70 | 36347 | | | 296 | 26.9 | 001/46 | 328.4 | 63.2 | Hungry Ridge | −6.6±61 |
| NHPC[b] | 39.78 | 119.55 | 8/10 | 26.7 | 10.2 | 28.7 | 25.7 | 305/38 | 29.1 | −12.1 | Paiute Creek | 54.0±9.4 |
| NHPR03[b] | 39.60 | 119.36 | 36325 | 164.6 | 5.2 | 4.2 | 56.9 | 146/25 | 319.5 | 64.4 | Painted Rock | −15.5±10.7 |
| NHSS01[b] | 39.74 | 119.69 | 36379 | 123.4 | 5.0 | 356.2 | 55 | 108/30 | 301.9 | 73.2 | Spanish Springs | −33.1±10.6 |
| NHWS1[b] | 39.76 | 119.57 | 9/ | | | 66.5 | 65.5 | 287/37 | 39.5 | 34.3 | Warm Spring V. | 64.5 |
| NHWS2[b] | 39.78 | 119.58 | 7/ | 100.8 | 6.0 | 18.4 | 43.2 | 205/16 | 4.8 | 39.1 | Warm Spring V. | 29.8±7.7 |
| *Basalt of Churchill Butte* | | | | | | | | | | | | |
| BCB01 | 39.31 | 119.34 | 36288 | 21.6 | 16.8 | 342.4 | 25.9 | 230/07 | 342.1 | 19 | Churchill Butte | −14.8±14.1 |
| BCB02 | 39.31 | 119.34 | 36226 | 5099.5 | 1.7 | 357.2 | 63.7 | 230/07 | 353.2 | 57.7 | Churchill Butte | −3.7±3.9 |
| BCB03 | 39.31 | 119.34 | 36380 | 60.4 | 5.2 | 30.5 | 37.8 | 230/07 | 26.6 | 33.5 | Churchill Butte | 29.7±5.7 |
| BCB04[b] | 39.31 | 119.34 | 36289 | 10.5 | 24.8 | 19.1 | 50.2 | 230/07 | 12.5 | 46.5 | Churchill Butte | 15.6 |
| BCB05 | 39.31 | 119.34 | 36224 | 45.8 | 11.4 | 31.2 | 57.1 | 230/07 | 23.4 | 52.7 | Churchill Butte | 26.5±14.6 |
| BCB06 | 39.31 | 119.34 | 36255 | 95.7 | 5.7 | 26.5 | 66.1 | 230/07 | 16.5 | 61.1 | Churchill Butte | 19.6±9.5 |
| BCB07 | 39.31 | 119.34 | 36255 | 151.4 | 5.5 | 24.6 | 56.5 | 230/07 | 17.8 | 51.5 | Churchill Butte | 20.9 |
| BCB08[b] | 39.31 | 119.34 | 36347 | 1.4 | 92.9 | 157.4 | 40.4 | 230/07 | 159.4 | 47 | Churchill Butte | −17.5 |
| BCB09 | 39.33 | 119.32 | 36255 | 113.0 | 5.7 | 16.4 | 70.7 | 230/07 | 6.5 | 65 | Churchill Butte | 9.6±10.7 |
| BCB10 | 39.33 | 119.32 | 36319 | 49.5 | 6.9 | 54.1 | 53.3 | 230/07 | 45.5 | 51.3 | Churchill Butte | 48.6±9.2 |
| BCB11 | 39.33 | 119.32 | 36258 | 100.2 | 5.2 | 51.4 | 64.8 | 230/07 | 38.2 | 62.2 | Churchill Butte | 41.3±9.1 |
| BCB12[b] | 39.30 | 119.32 | 36349 | 1.4 | 89.7 | 130.6 | −8.4 | 230/07 | 130.7 | −1.7 | Churchill Butte | −46.2 |
| BCB13[b] | 39.3 | 119.32 | 36411 | 1.6 | 62.4 | 2.3 | 64.7 | 230/07 | 354.1 | 59.4 | Churchill Butte | −2.8 |
| BCB14[b] | 39.30 | 119.32 | 36256 | 3.0 | 64.7 | 298.5 | −43 | 230/07 | 295.6 | −49.5 | Churchill Butte | −61.3 |
| Average | | | 36416 | 16.0 | 4.5 | | | | 21.2 | 51.3 | | 24.3±6.5 |

Table 1 (*continued*)

| Site | Lat. °W | Long.°N | $N/N_o$ | $\kappa$ | $\alpha_{95}$ | *Dg* | *Ig* | *St/Dp* | *Ds* | *Is* | Locality | Rotation |
|---|---|---|---|---|---|---|---|---|---|---|---|---|
| *Basalt of Cleaver Peak* | | | | | | | | | | | | |
| BCP01 | 39.20 | 119.18 | 36255 | 31.9 | 10.9 | 30.3 | 49.6 | 184/03 | 027.0 | 50.9 | Cleaver Peak | 30.1±13.6 |
| BCP02 | 39.20 | 119.18 | 36319 | 61.0 | 5.9 | 39.8 | 41.6 | 184/03 | 037.6 | 43.4 | Cleaver Peak | 40.7±7 |
| BCP03 | 39.20 | 119.18 | 36348 | 79.9 | 5.1 | 58.6 | 46.5 | 184/03 | 56.7 | 48.9 | Cleaver Peak | 59.8±6.8 |
| BCP04 | 39.20 | 119.18 | 36380 | 298.5 | 3.2 | 67.9 | 37.4 | 184/03 | 066.8 | 40.1 | Cleaver Peak | 69.9±4.8 |
| BCP05 | 39.20 | 119.18 | 36411 | 465.0 | 2.4 | 39.8 | 45.1 | 184/03 | 037.2 | 46.8 | Cleaver Peak | 40.3±4.1 |
| BCP06 | 39.21 | 119.18 | 36319 | 173.2 | 3.9 | 40 | 43.2 | 184/03 | 037.6 | 45 | Cleaver Peak | 40.7±5.3 |
| BCP07 | 39.21 | 119.18 | 36411 | 207.8 | 3.6 | 22 | 43.4 | 184/03 | 029.4 | 44.7 | Cleaver Peak | 32.5±5 |
| BCP08 | 39.20 | 119.18 | 36316 | 488.5 | 3.0 | 64.7 | 47.2 | 184/03 | 063.0 | 49.8 | Cleaver Peak | 66.1±4.7 |
| BCP09 | 39.20 | 119.18 | 36316 | 297.5 | 2.5 | 64.7 | 44 | 184/03 | 63.2 | 46.6 | Cleaver Peak | 66.3±4.2 |
| BCP10 | 39.20 | 119.18 | 36316 | 221.2 | 4.5 | 66.2 | 42.9 | 184/03 | 064.9 | 45.5 | Cleaver Peak | 68±5.9 |
| BCP11 | 39.20 | 119.18 | 36285 | 164.5 | 6.0 | 59.2 | 46.7 | 184/03 | 058.0 | 49.5 | Cleaver Peak | 61.1±7.8 |
| Average | | | 36474 | 49.4 | 2.1 | | | | 51.2 | 47.7 | | 54.3±3.9 |
| *Basalt of Silver Spring* | | | | | | | | | | | | |
| BSSN01 | 39.47 | 119.23 | 36442 | 375.5 | 1.6 | 224.5 | −56.2 | 330/01 | 224.9 | −56.2 | Silver Spring | 48±3.8 |
| BSSN02 | 39.47 | 119.23 | 36348 | 145.6 | 3.3 | 203.9 | −66 | 330/01 | 205.3 | −66 | Silver Spring | 28.4±7.0 |
| BSSN03 | 39.47 | 119.23 | 36320 | 37.2 | 6.6 | 200.6 | −53 | 330/01 | 201.4 | −53 | Silver Spring | 24.5±9.1 |
| BSSN04 | 39.47 | 119.23 | 36411 | 40.9 | 5.6 | 221.4 | −49.9 | 330/01 | 221.8 | −49.9 | Silver Spring | 44.9±7.5 |
| BSSN05 | 39.47 | 119.23 | 36379 | 146.0 | 2.7 | 233.9 | −56.8 | 330/01 | 234 | −57.8 | Silver Spring | 57.1±4.9 |
| BSSN06 | 39.47 | 119.23 | 36379 | 342.2 | 2.1 | 243.6 | −68.5 | 330/01 | 243.4 | −67.5 | Silver Spring | 66.5±5.1 |
| BSSN07 | 39.47 | 119.23 | 36255 | 106.9 | 4.2 | 246.6 | −53.3 | 330/01 | 245.9 | −53.3 | Silver Spring | 69±6.2 |
| BSSN08[b] | 39.47 | 119.23 | 36316 | 1.8 | 47.8 | 188.4 | −24.7 | 330/01 | 188.8 | −24.7 | Silver Spring | 11.9±42.7 |
| BSSN09[c] | 39.47 | 119.23 | 36316 | | | 233.4 | −72.5 | 330/01 | 233.8 | −72.5 | Silver Spring | 56.9±9.6 |
| BSSN10 | 39.47 | 119.23 | 36316 | 157.9 | 2.9 | 193.4 | −69.1 | 330/01 | 195.3 | −69.1 | Silver Spring | 18.4±7.1 |
| BSSN11 | 39.47 | 119.23 | 36316 | 97.4 | 4.2 | 198.1 | −75 | 330/01 | 200.6 | −75 | Silver Spring | 23.7±13.2 |
| BSSN12 | 39.47 | 119.23 | 36255 | 67.7 | 6.8 | 201.9 | −60.4 | 330/01 | 203 | −60.4 | Silver Spring | 26.1±10.8 |
| BSSN13 | 39.47 | 119.23 | 36257 | 66.4 | 6.9 | 255.3 | −67 | 330/01 | 255.3 | −67.4 | Silver Spring | 78.4±13.9 |
| BSSN17 | 39.47 | 119.21 | 36319 | 276.3 | 4.0 | 257.2 | −73.8 | 330/01 | 256.1 | −73.8 | Silver Spring | 79.2±11.7 |
| BSSN18 | 39.47 | 119.21 | 36442 | 87.5 | 3.5 | 241.2 | −67 | 330/01 | 239.3 | −67 | Silver Spring | 62.4±7.7 |
| BSSN19 | 39.46 | 119.22 | 36443 | 127.0 | 4.3 | 204.4 | −30.8 | 330/01 | 204.7 | −30.8 | Silver Spring | 27.8±5 |
| Average | | | 15/16 | 25.3 | 2.1 | | | | 222.2 | −61.5 | | 45.3±4. |
| *Basalt of Oxbow Canyon* | | | | | | | | | | | | |
| BOX01[b] | 39.60 | 119.46 | 8/8 | 1.8 | 59.8 | 174.1 | 24.1 | 207/15 | 181 | 31.4 | Oxbow Canyon | −179 |
| BOX02 | 39.60 | 119.46 | 11/11 | 35.7 | 7.8 | 257.3 | −53.8 | 207/15 | 238.6 | −63.9 | Oxbow Canyon | 61.7±14.5 |
| BOX03 | 39.6 | 119.46 | 36285 | 12.5 | 15.1 | 242.4 | −46.6 | 207/15 | 232.6 | −51.6 | Oxbow Canyon | 55.7±10 |
| BOX04[b] | 39.60 | 119.46 | 36411 | 189.5 | 2.6 | 103.9 | 48 | 207/15 | 96 | 61.8 | Oxbow Canyon | −80.9±5.3 |
| BOX05 | 39.60 | 119.46 | 6/6 | 73.1 | 7.9 | 224.7 | −51.8 | 207/15 | 204.9 | −54 | Oxbow Canyon | 28±11 |
| BOX06 | 39.60 | 119.46 | 9/9 | 196.3 | 3.7 | 227.5 | −49.9 | 207/15 | 208.9 | −53 | Oxbow Canyon | 32±5.7 |
| BOX07 | 39.60 | 119.46 | 7/7 | 200.9 | 4.3 | 237.3 | −55.1 | 207/15 | 214.6 | −60.3 | Oxbow Canyon | 37.7±7.5 |
| BOX08 | 39.60 | 119.46 | 7/7 | 405.4 | 3.0 | 226 | −49.1 | 207/15 | 207.9 | −51.9 | Oxbow Canyon | 31±4.9 |
| BOX09 | 39.60 | 119.46 | 7/7 | 249.7 | 3.8 | 236.9 | −56 | 207/15 | 213.4 | −60.9 | Oxbow Canyon | 36.5±6.8 |
| BOX10 | 39.60 | 119.46 | 36347 | 978.1 | 1.5 | 234.5 | −54.3 | 207/15 | 212.5 | −58.9 | Oxbow Canyon | 35.6±3.8 |
| BOX11 | 39.60 | 119.45 | 8/8 | 352.5 | 3.0 | 226 | −50.7 | 207/15 | 206.9 | −53.4 | Oxbow Canyon | 30±4.9 |
| BOX12 | 39.60 | 119.45 | 36347 | 283.8 | 3.6 | 223.7 | −56.1 | 207/15 | 200.8 | −57 | Oxbow Canyon | 23.9±0.6 |
| BOX13 | 39.60 | 119.45 | 5/5 | 216.2 | 5.2 | 246.6 | −52.4 | 207/15 | 227 | −60.2 | Oxbow Canyon | 50.1±8.6 |
| BOX14 | 39.60 | 119.45 | 36379 | 582.7 | 2.3 | 241.1 | −47.4 | 207/15 | 224.5. | −54.2 | Oxbow Canyon | 47.6±4.3 |
| BOX15 | 39.60 | 119.45 | 36411 | 642.2 | 1.5 | 243.3 | −51.5 | 207/15 | 224.1 | −58.4 | Oxbow Canyon | 47.2±3.8 |
| BOX16 | 39.60 | 119.45 | 36222 | 1360.5 | 2.5 | 238.4 | −48.8 | 207/15 | 220.6 | −54.8 | Oxbow Canyon | 43.7±4.5 |
| BOX17 | 39.60 | 119.45 | 8/8 | 551.9 | 2.2 | 244.8 | −54.8 | 207/15 | 222.9 | −61.8 | Oxbow Canyon | 46±4.8 |
| Average | | | 15/17 | 24.0 | 2.6 | | | | 219 | −56.1 | | 42.1±4.8 |

Table 1 (*continued*)

| Site | Lat. °W | Long.°N | $N/N_o$ | $\kappa$ | $\alpha_{95}$ | *Dg* | *Ig* | *St/Dp* | *Ds* | *Is* | Locality | Rotation |
|---|---|---|---|---|---|---|---|---|---|---|---|---|
| *Basalt of Vista* | | | | | | | | | | | | |
| BV01 | 39.54 | 119.67 | 36227 | 44.9 | 10.1 | 034.4 | 51.6 | 155/08 | 025.7 | 56.7 | Vista | 28.8±14.3 |
| BV02 | 39.54 | 119.67 | 36258 | 210.6 | 3.9 | 032.8 | 49.6 | 155/08 | 025.9 | 49.6 | Vista | 29±5.5 |
| BV03 | 39.54 | 119.67 | 36411 | 373.3 | 2.7 | 033.0 | 42.6 | 155/08 | 026.7 | 47.8 | Vista | 29.8±4.4 |
| BV04 | 39.54 | 119.67 | 36349 | 502.6 | 2.7 | 014.6 | 44.6 | 155/08 | 006.7 | 47.6 | Vista | 9.8±4.4 |
| BV05 | 39.54 | 119.67 | 36258 | 87.4 | 6.5 | 024.7 | 33.2 | 155/08 | 019.0 | 37.3 | Vista | 22.1±6.9 |
| BV06 | 39.54 | 119.67 | 36319 | 70.1 | 5.2 | 024.0 | 49.3 | 155/08 | 015.2 | 53.1 | Vista | 18.3±7.5 |
| BV07 | 39.54 | 119.57 | 36199 | 58.9 | 12.1 | 016.2 | 48.6 | 155/08 | 007.2 | 51.5 | Vista | 10.3±14.1 |
| BV08 | 39.54 | 119.57 | 36199 | 518.5 | 4.8 | 016.4 | 33.5 | 155/08 | 011.2 | 36.6 | Vista | 14.3±5.2 |
| BV09 | 39.54 | 119.57 | 36380 | 41.5 | 6.0 | 001.5 | 44.5 | 155/08 | 353.6 | 45.4 | Vista | −3.3±7.3 |
| BV10 | 39.54 | 119.57 | 36349 | 115.0 | 3.9 | 351.7 | 47.9 | 155/08 | 343.0 | 47.3 | Vista | −13.9±5.4 |
| BV11[b] | 39.54 | 119.57 | 36258 | 12.4 | 27.1 | 313.9 | 38.2 | 155/08 | 309.5 | 33.1 | Vista | −47.4±4 |
| Average | | | 10/11 | 32.2 | 2.8 | | | | 008.3 | 48.6 | | 11.4±4.4 |

[a] Key: site is site name; Lat.°W and Long.°N are site latitude and longitude; $N/N_o$ is the number of samples accepted/number of samples demagnetized; $\alpha_{95}$ is 95% confidence cone about mean; *Dg* and *Ig* are declination and inclination of site mean direction in geographic coordinates; *St/Dp* are strike and dip at site (dip direction 90° clockwise from strike); *Ds* and *Is* are declination and inclination of site mean direction in stratigraphic coordinates; rotation is estimate of vertical-axis rotation of site relative to average direction for individual flows. Site mean and $\alpha_{95}$ derived using Fisher statistics. Average is unit mean of multiple sites for a given locality.

[b] Sites gave anomalous results.

[c] $\alpha_{95}$ calculated using Bingham statistics and give confidence angles: alpha 3-1 = 3.56 and alpha 3-2 = 16.38.

were calculated using the statistics of Fisher (1953).

The magnetic mineralogy of the Nine Hill tuff indicates that it is a stable recorder of mid-Tertiary paleomagnetism. Magnetic mineralogy was evaluated for most sites through interpretation of both demagnetization curves and hysteresis analysis; in some cases, SIRM acquisition was also measured (Fontaine, 1997). Thermal demagnetization curves indicate that in most cases, the specimens had lost at least 75% of their original magnetization by 550°C, and in all cases, magnetization had been reduced to $J/J_0 < 0.10$ by 600° C. This suggests that the primary magnetic mineral is close to pure magnetite, with some oxidation to maghemite. A small percentage of magnetization commonly remains at the end of the demagnetization series, suggesting that a minor amount of hematite is also present. When measured, SIRM acquisition was ca. 600 mT. This is above the saturation level expected for pure magnetite (300 mT), but well below that expected for hematite (3 T), and is consistent with the presence of maghemite. Hysteresis plots also support this interpretation (Fig. 4): The magnetic species is typically single-domained and is primarily composed of ferrimagnetic material, probably magnetite or maghemite, with minor components of diamagnetic and paramagnetic materials.

Paleomagnetic data obtained from tuffs are used differently than are those from basalts to determine tectonic rotations. The Nine Hill tuff is a single widespread volcanic unit. It acquired its magnetization quickly, and therefore captured a spot reading of the geomagnetic field. Paleomagnetic analyses from a number of widely scattered Nine Hill tuff localities throughout the Sierra Nevada (see next paragraph) have established that the reference direction of the Nine Hill tuff is declination 335°, inclination 58° (Deino, 1985). Remanent directions from Nine Hill tuff sites elsewhere can be compared to this reference direction to determine tectonic rotations. Localities with inclinations very different from that of the reference direction reflect either multiple rotations, rotation about an inclined axis, or an error in determining paleohorizontal, and therefore cannot confidently be used as indicators of vertical-axis rotation. We used the method of Vandamme (1994) to identify the optimum cutoff for such samples, thus excluding sites

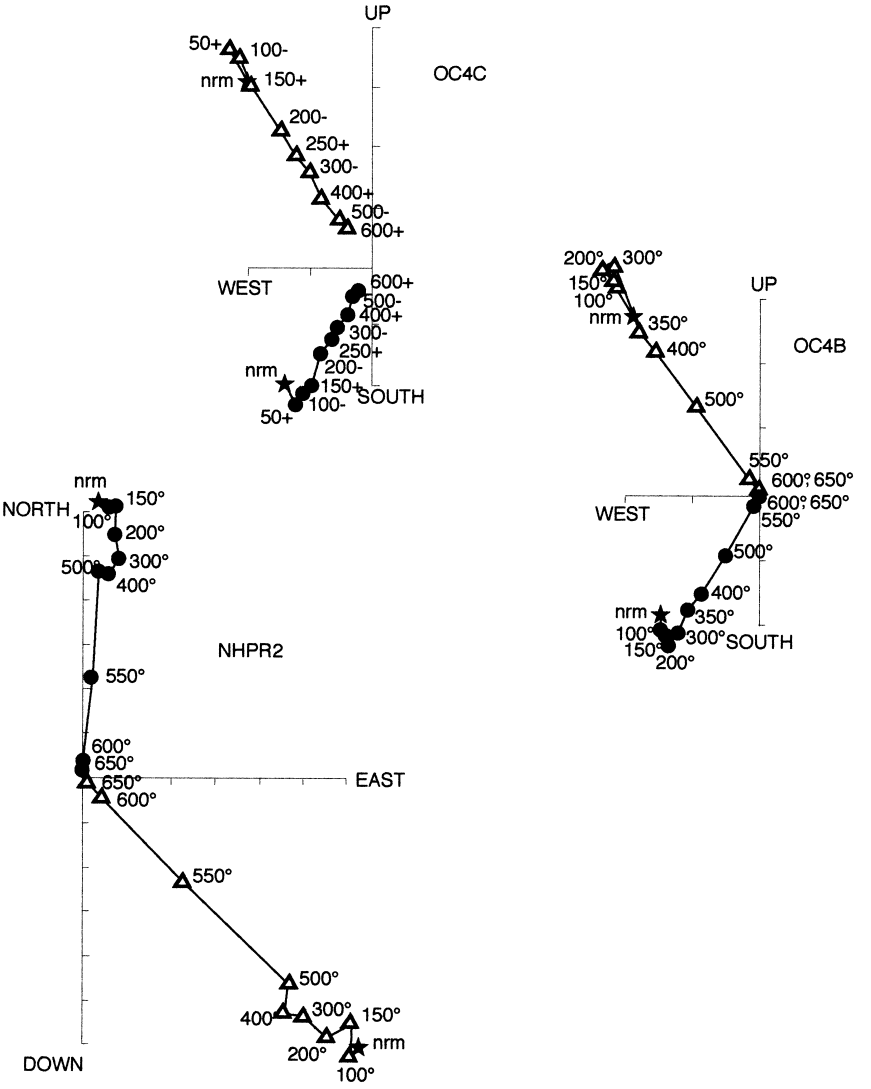


Fig. 3. Orthogonal progressive demagnetization diagrams for representative Nine Hill tuff and basalt samples. Axes are in stratigraphic coordinates. The diagram for the Nine Hill tuff shows thermal demagnetization of specimen NHPR2, from the Carson domain. Specimens OC4B and OC4C are from a single basalt sample, also from the Carson domain and illustrate the comparison between thermal and alternating field demagnetization for these rocks. Note that reverse polarity magnetizations were recorded at this site. Inclinations for each demagnetization step are shown by triangles, on two-dimensional cross-sectional coordinates. Declinations for each step are shown by circles, on two-dimensional map-view coordinates. Both decrease in intensity toward the origin of the plot. Map locations for all samples are shown in Fig. 7.

where the inclination was more than 16.5° above or below the reference inclination. For basalts, in contrast, a reference direction is not known for each individual basalt flow. Therefore, a number of temporally discrete flows from a given locality must be used to average paleosecular variation. The average remanent direction from each locality can then be compared to the reference field direction at the time the basalt flows cooled, in order to determine tectonic rotations. A Neogene refer-

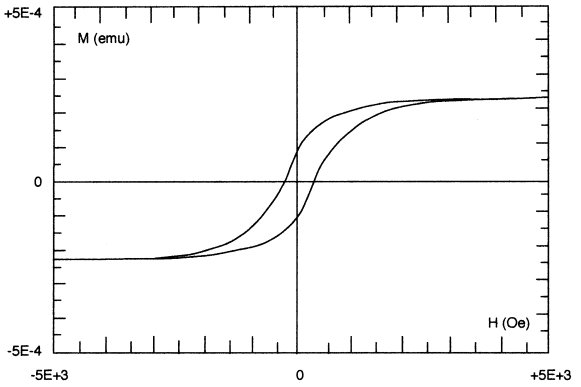


Fig. 4. Representative hysteresis plot for the Nine Hill tuff; specimen NHPAa shown. $H_c = 293$ Oe, $M_r = 93.7$ μemu, $M_s = 228$ μemu, $M_r/M_s = 0.411$, slope correction $= -1.61$ μemu Oe$^{-1}$, slope correction $= -1.61$ nemu Oe$^{-1}$. $H_c$, Specimen coercivity; $M_r$, specimen remanent magnetism; $M_s$, specimen saturation magnetization; $M_r/M_s$ indicates relative domain structure: 0.5 is single-domained, 0.01 is multi-domained.

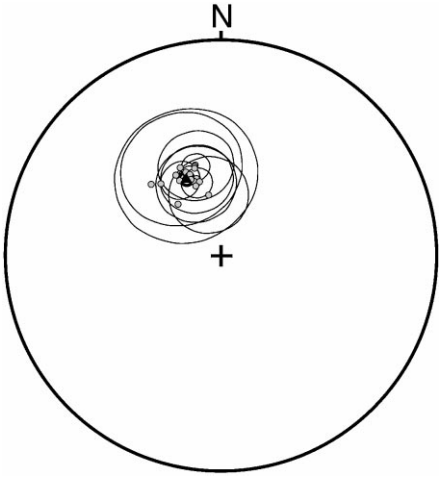


Fig. 5. Reference direction for the Nine Hill tuff from Deino (1985). Samples are from 17 sites in the central Sierra Nevada and four sites in western Nevada. Deleting the Nevada sites changes the reference direction by $<1°$ (see text). ○, Individual site means; ▲, reference direction.

ence pole from Hagstrom (1987) was used for the Neogene basalts in this study.

The reference direction for the Nine Hill tuff was determined primarily from localities in the central Sierra Nevada, not the Walker Lane; paleomagnetic studies of the Nine Hill tuff in the Walker Lane therefore measure tectonic rotations relative to the Sierra block. Deino (1985) used the paleomagnetic signature of the Nine Hill tuff as an independent check on the correlation of the tuff in its more distal exposures in the central Sierra Nevada. In his study, he used 57 samples from 21 sites, and calculated a reference direction of declination = 335.1°, inclination = 57.5° (Fig. 5). All but four of these sites are in the Sierra; they cover a geographic range of ca. 120 km, from Calaveras Co. (120 km SW of Carson City) in the south to Sierra Co. (50 km WNW of Carson City) in the north. The other four sites Deino (1985) sampled are from western Nevada, and all are sites we sampled for this study. They are Red Rock Canyon, Red Rock Valley (equivalent to our Porcupine Mountain), Santiago Canyon and Warm Springs Valley. Deino's Warm Springs Valley site had a strongly anomalous direction (as did our samples from the same area, NHWS1, NHWS2, NHCRE, NHPC and most samples from NHRC; see Results, below, and Table 1), and was therefore excluded from his calculation of reference direction. When we recalculate the reference direction excluding the remaining three sites (thus using only sites in the Sierra), the declination changes 0.8 to 335.9°, and the inclination remains 57.5°.

Both the Nine Hill tuff and the basalts used in this study typically responded to progressive demagnetization in a fairly simple manner (Fig. 3). After weak secondary components are removed by the initial demagnetization steps, most samples of both tuff and basalt carry one dominant magnetization that is thought to have been acquired during initial cooling. Specimens that did not exhibit univectorial decay of remanence or that showed demagnetization characteristics very different than the other specimens from the same site were not used in calculations of the site mean direction. Lightning-induced isothermal remanent magnetizations have overprinted the characteristic magnetization at some sites. These are recognized by their high magnetic moments, low resistance to alternating field demagnetization, dispersed directions and, frequently, by local anomalies measurable in the field using a hand-held compass. Lightening-overprinted sites were also omitted from calculations.

## 4. Results

### 4.1. Pyramid Lake domain

Tilt-corrected paleomagnetic orientations in the Nine Hill tuff were compared to the reference direction to evaluate possible vertical-axis rotation in the Pyramid Lake domain. Most sampling sites were selected from the detailed study of the Nine Hill tuff by Deino (1985); he used chemical analyses to confirm the presence of the tuff at these sites. No other rock types were studied in the Pyramid Lake domain, because exposures of Nine Hill tuff are well distributed throughout the domain, and because the overall lack of rotation (see below) made investigation of rotation rates unnecessary.

Nine Hill tuff samples from the structural blocks bounded by the major northwest-striking faults are unrotated or show slight counter-clockwise (CCW) rotation (Figs. 6 and 7; Table 1). One of these sites (NHMP) is from the Virginia Range between the Pyramid Lake fault and the Warm Spring Valley fault, three (NHMS, NHFS and NHPA) are from three ranges between the Warm Springs Valley fault and all splays of the Honey Lake fault, and two (NHRR and NHPM) are between two splays of the Honey Lake fault. Of these six sites, two are statistically indistinguishable from the unrotated reference direction, and the other four show CCW rotations of 12–24°.

In striking contrast to samples from within the fault-bounded blocks, Nine Hill tuff samples taken close to the major dextral faults show varying but significant amounts (30–60°) of clockwise (CW) vertical-axis rotation, which we attribute to drag during faulting (Figs. 6–7; Table 1). In southern Warm Springs Valley, near the southern termination of the Warm Springs Valley fault, the Oligocene–Miocene tuff section is faulted and broadly folded within 2 km of the fault (Garside et al., 1999). The geometry of the folding is consistent with drag along a dextral fault. We sampled the Nine Hill tuff at five sites along a traverse perpendicular to the fault, to test whether rotation increased approaching the fault. Unfortunately, a strong secondary magnetic overprint has obliterated the primary remanent direction in this area. Four of the five sites (NHCRE, NHPC, NHWS1, NHWS2) were unusable, and only a few samples from the fifth site (NHRC) retained a measurable primary remanent magnetization. These showed substantial CW rotation (Table 1). Elsewhere, the major dextral faults underlie the alluvium in the valleys, and our sampling has been limited to tuff exposures low on the flanks of the ranges, within a few kilometers of the faults. These sites (NHMC, NHSL and NHTC) all exhibit 30–40° CW rotation, in contrast to the unrotated, or slightly CCW rotated, samples from the interiors of the same ranges. By analogy with the well-exposed, broadly folded tuff adjacent to the Warm Springs Valley fault, we attribute the CW rotations from the edges of the ranges to drag along the dextral faults in the valleys.

Nine Hill tuff samples from the region west of the Walker Lane, that is, between the northwest-

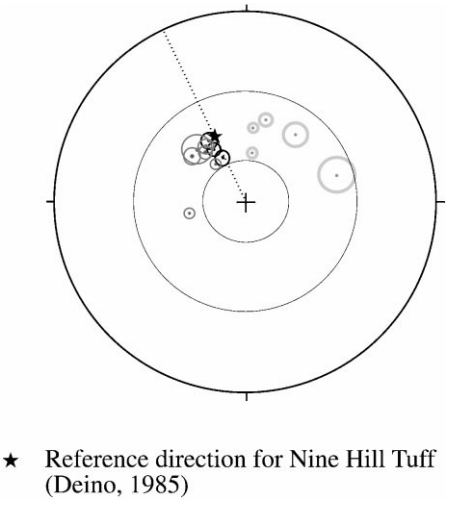


Fig. 6. Summary stereographic plot of vertical-axis rotations in the Pyramid Lake domain, showing measured orientations (corrected for stratigraphic dip) and $\alpha_{95}$ confidence cones. All rotations in this domain were measured in the Nine Hill tuff. The dotted line shows the reference declination of the Nine Hill tuff and circles show the reference inclination $\pm 16°$. Statistically unrotated sites are shown in black, sites with counter-clockwise rotation in gray (fine lines) and sites with clockwise rotation in light gray (thick lines). Four of the latter sites (NHRC, NHMC, NHTC and NHSL) are adjacent to one of the domain-defining dextral faults and the clockwise rotation is attributed to drag along these faults; the fifth (NHHR) is from the extensional domain between the Walker Lane and the Sierra.

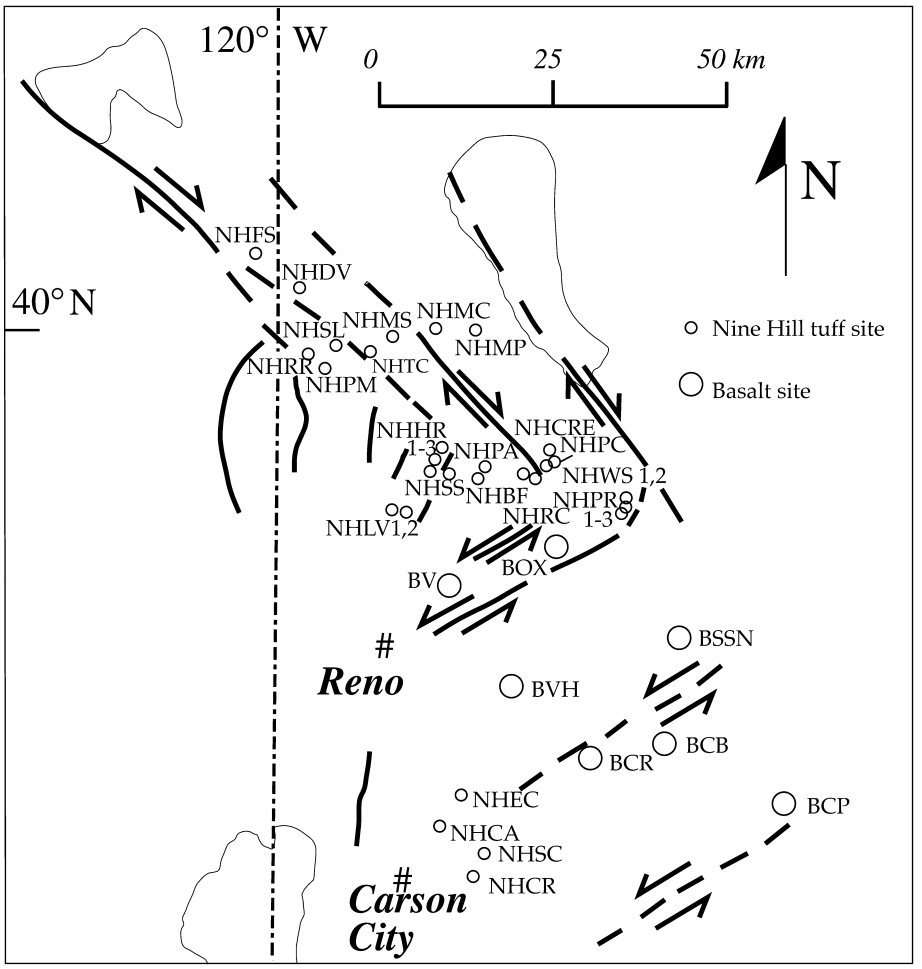


Fig. 7. Map showing locations of all paleomagnetic samples included in Table 1. (Note that all samples are shown here, even those that did not yield usable results and are therefore not included on the summary map in Fig. 9.)

striking faults and the Sierra Nevada, give inconsistent vertical-axis rotations (Figs. 6 and 7; Table 1). This region is characterized by north-striking normal faults, most of which have Pleistocene to Holocene motion (Bell, 1984). Exposures of Nine Hill tuff are limited, and usable results were obtained only from one site on the northeast end of Hungry Ridge (NHHR1) and from two sites in Lemmon Valley (NHLV1 and NHLV2), on the southwest flank of Hungry Ridge. Tilt-corrected paleomagnetic orientations for these three sites include unrotated and strongly rotated both CW and CCW (Figs. 6 and 7; Table 1). These unsystematic results, and comparable variability at several unusable sites from the same area (NHHR2, NHHR3 and NHSS), suggest that more than just a single vertical-axis rotation may be involved; the numerous faults mapped in both areas (Bonham, 1969; Cordy, 1985) could explain the multiple motions.

### 4.2. Carson domain

Tilt-corrected paleomagnetic orientations in the Nine Hill tuff and in younger basalts were compared to their reference directions to evaluate

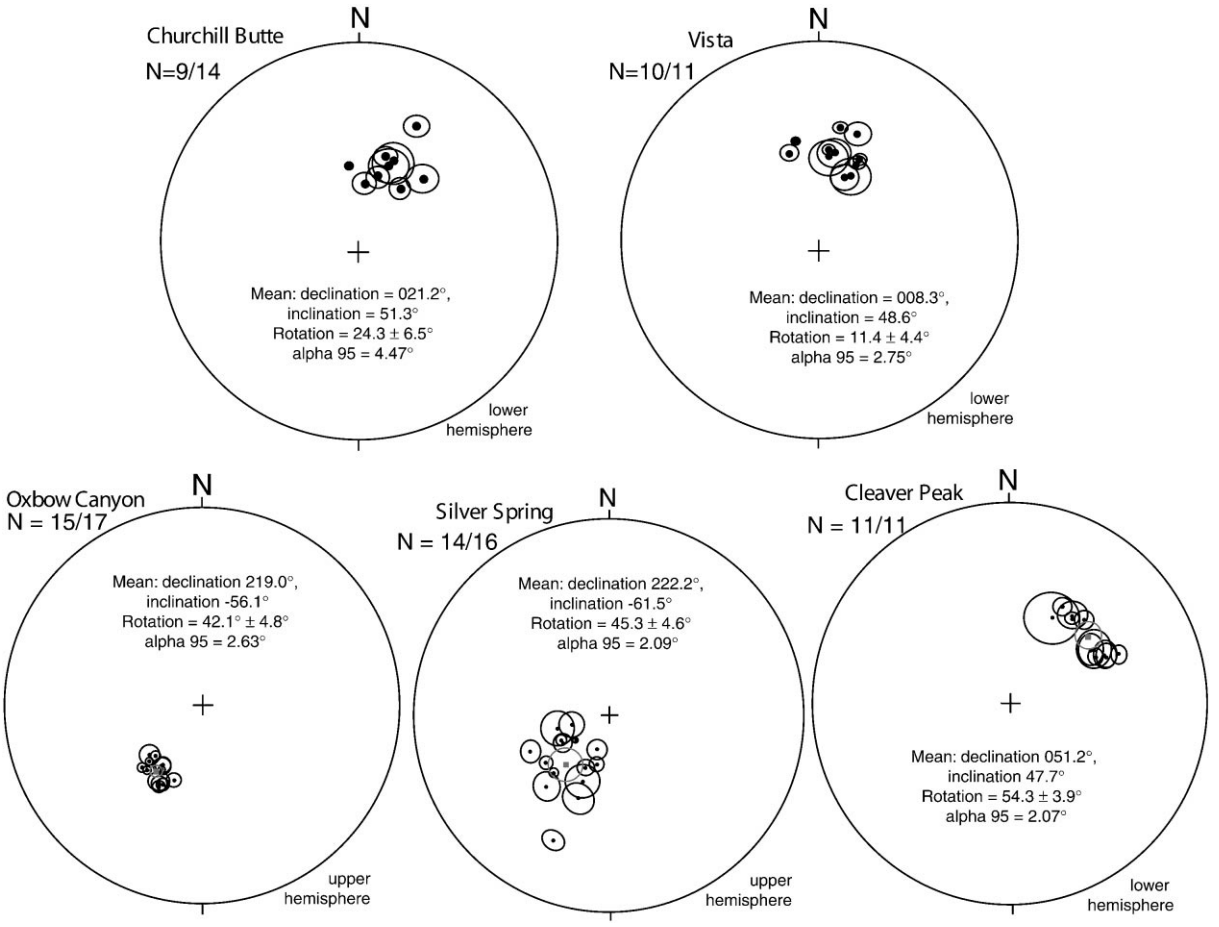


Fig. 8. Equal-area projections showing tilt-corrected mean remanence directions for basalt localities from the Carson domain. ●, mean direction for each site (flow), in circle, 95% confidence cone. *N*, number of flows used, compared to number of flows sampled, at each locality. ■, Mean for the locality, using data from all sites, in circle = 95% confidence cone. Two localities (Oxbow Canyon and Silver Spring) have reverse polarities and are shown on upper hemisphere plots.

possible vertical-axis rotation in the Carson domain (Figs. 7 and 8; Table 1). The depth of erosion in the Carson domain as a whole is significantly less that in the Pyramid Lake domain, so there are few exposures of the Oligocene–Miocene tuffs, and virtually no exposures of pre-Tertiary crystalline rocks. Usable outcrops of Nine Hill tuff were found in only a few places. Younger basalts, initially chosen to provide a better geographic distribution of rotation data, also provide the opportunity to constrain both timing and rate of rotation in the Carson domain. Several criteria were used to select basalt sampling sites:

1. radiometric age control;
2. presence of multiple flows, so paleosecular variation could be averaged;
3. evidence of paleohorizontal; and
4. geographic distribution.

The clockwise sense of rotation we measured is consistent throughout the Carson domain. We found no evidence (either structural or paleomagnetic) of drag folding near faults like that found

in the Pyramid Lake domain. Note that drag folding results in *counter*-clockwise rotation adjacent to sinistral faults, such as those that define the Carson domain. We found no counter-clockwise rotation in the Carson domain.

#### 4.2.1. Nine Hill tuff

Nine Hill tuff from two sites at Painted Rock (NHPR1 and NHPR2), in the northeastern corner of the domain, records 35–44° of clockwise vertical-axis rotation (Figs. 6 and 7; Table 1). These results are consistent with rotations measured in basalts throughout the domain (see below). They are therefore interpreted to be representative of deformation in the Carson domain. Nine Hill tuff from two sites near Carson City (NHCA and NHSC) is statistically unrotated (Figs. 6 and 7; Table 1); these sites are interpreted to be west of the Carson domain, that is, west of the Walker Lane.

#### 4.2.2. 9–13 Ma basalts

Basalts 9–13 Ma in age from three localities spanning the north–south extent of the Carson domain record 42–54° of clockwise vertical-axis rotation (Figs. 7 and 8; Table 1). Two of these localities, one northwest of Silver Springs (BSSN) and one near Cleaver Peak north of Wabuska (BCP), have whole-rock ages of $11.8 \pm 0.7$ and $9.2 \pm 0.6$ Ma, respectively (Stewart et al., 1994). The third, at Oxbow Canyon on the north side of the Truckee River (BOX), is not dated, but is along strike from a section within the Pyramid basalt including $13.3 \pm 0.7$ Ma andesite or basalt, and $11.7 \pm 0.4$ Ma rhyolite tuff [both are K/Ar dates on biotite (Stewart et al., 1994)], so is thought to be ca. 12–13 Ma. Eleven to 16 individual flows (sites) were sampled at each locality, and the results for each averaged, to remove the effects of paleosecular variation. The similar rotation amounts in spite of the opposite polarities recorded by these sites (normal for Oxbow and reversed for Silver Springs and Cleaver Peak) suggests that the sites have adequately averaged paleosecular variation. The similarity of rotations over such widely spaced sampling localities also suggests that large blocks have rotated in the Carson domain. There is no evidence of increasing rotation with proximity to block-bounding faults, which has been interpreted elsewhere (e.g. Nelson and Jones, 1987) to show smaller, independently-rotating blocks.

#### 4.2.3. 4–7 Ma basalts

The large rotations in 9–13 Ma basalts of the Carson domain gave us confidence that tectonic rotations might be resolvable in younger rocks. Basalts and olivine-bearing basaltic andesites at Churchill Butte (BCB), in the south-central part of the domain, are dated as $4.3 \pm 0.6$, $3.5 \pm 0.2$ and $3.3 \pm 0.2$ Ma (Stewart et al., 1994), and record $24.3 \pm 6.5°$ of clockwise rotation (Figs. 7 and 8, Table 1). An undated site mapped as 5–7 Ma Lousetown basalt near Vista (Bell and Bonham, 1987), in the northwestern corner of the domain, has a $11.4 \pm 4.4°$ CW rotation. Two additional sites did not provide usable results: rocks at the Chavez Ranch site, west of Churchill Butte, are not stable recorders of remanence, most likely because of rapid quenching. Basalts from the type locality of the 5–7 Ma Lousetown basalt, north of Virginia City, record an anomalous orientation (declination northeast, with a *negative* inclination). This appears to be a transient field orientation, as also noted by Henrichs (1967), and is therefore not useful for determining vertical-axis rotation.

## 5. Kinematic model–strain partitioning in the northern Walker Lane

Our new data suggest that the dextral slip in the northern Walker Lane is partitioned into domains dominated by translation, rotation and extension. A kinematic model consistent with both the field relationships and the paleomagnetic results (Figs. 9 and 10) builds directly on Stewart's (1988) recognition of structural domains defined by the orientation of map-scale faults. Dextral slip in the Pyramid Lake domain occurs by translation along several major northwest-striking faults or fault zones. Farther west, between these faults and the present edge of the Sierra Nevada, there is a domain dominated by extension across north-striking normal faults. In contrast, dextral slip in the Carson domain occurs by clockwise rotation of

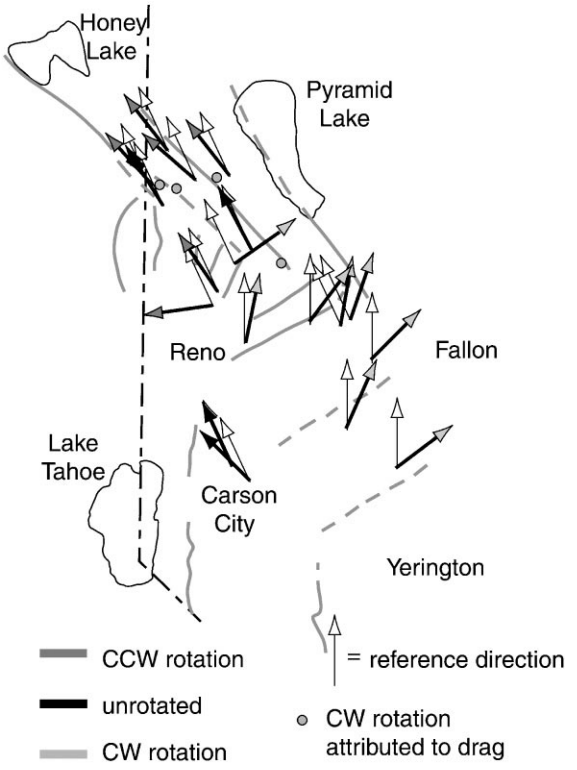


Fig. 9. Summary map of vertical-axis rotations (corrected for stratigraphic dip) in the northern Walker Lane. Each measured direction is compared to a reference direction; note that a different reference direction applies for basalts than for the Nine Hill tuff. For clarity, the four clockwise-rotated sites adjacent to faults the Pyramid Lake domain are shown as filled circles.

fault-bounded blocks. The domain-defining east-northeast-striking sinistral faults are probably the boundaries of these rotating blocks. An extensional domain also occurs between the Carson domain and the present Sierra Nevada frontal fault system. The deformation style we document in the Carson domain has not been described at this scale elsewhere in the Walker Lane. For the kinematic model, the dextral slip across the northern Walker Lane was arbitrarily set at 30 km, the minimum estimated by Bonham (1969, and personal communication, 1993). More (or less) dextral offset can be accommodated by changing the slip on individual faults, the number of faults, the dimensions of the rotating blocks, etc.

For the kinematic model, the slip in the Pyramid Lake domain was divided evenly between the three major dextral faults. It is also possible to model different amounts of slip on these faults; this would change the locations of the ends of the blocks, but would not significantly change the model. Minimum dimensions of the blocks are established by the present surface exposures of Mesozoic plutonic rocks and Oligocene–Miocene tuffs. Our paleomagnetic studies document slight CCW rotations of the fault-bounded blocks in the Pyramid Lake domain. [Note that even though two of six such localities are statistically unrotated (Fig. 6; Table 1), the mean declinations of both are CCW of the reference direction.] This rotation suggests that there has been a component of extension in addition to the dextral slip across this part of the Walker Lane, that is, that the Sierra Nevada is moving away from the Basin and Range in a direction that is more westerly than, rather than parallel to, the faults in the northern Walker Lane. The translating fault-bounded blocks have therefore been free to rotate slightly, because they are not constrained by the boundary of the rigid Sierra block to the west. An alternate possibility — that the reference direction for the Nine Hill tuff is actually somewhat west of the direction determined by Deino (1985) — is here thought to be less likely, given the multiple lines of evidence that there has been extension along the eastern edge of the Sierra (and west of the Walker Lane) since Mio-Pliocene time (see reference to Neogene basins, topographic laws and gravity laws, below).

For the kinematic model, the structural blocks of the Carson domain rotate around pivot points in the centers of their eastern margins. Changing the positions of these pivot points would change the positions of the blocks, or the relationship between the length of blocks, amount of rotation and total slip across the domain, but would not change the basic model. The similar amounts of rotation for the widely separated sampling sites in the Carson domain are consistent with a model of a few large blocks rather than numerous, independently rotating blocks. Space problems require that there be a component of extension across this part of the Sierra Nevada-Basin and Range boundary, as well; otherwise, compressional deformation would be expected at the southwest corners of the

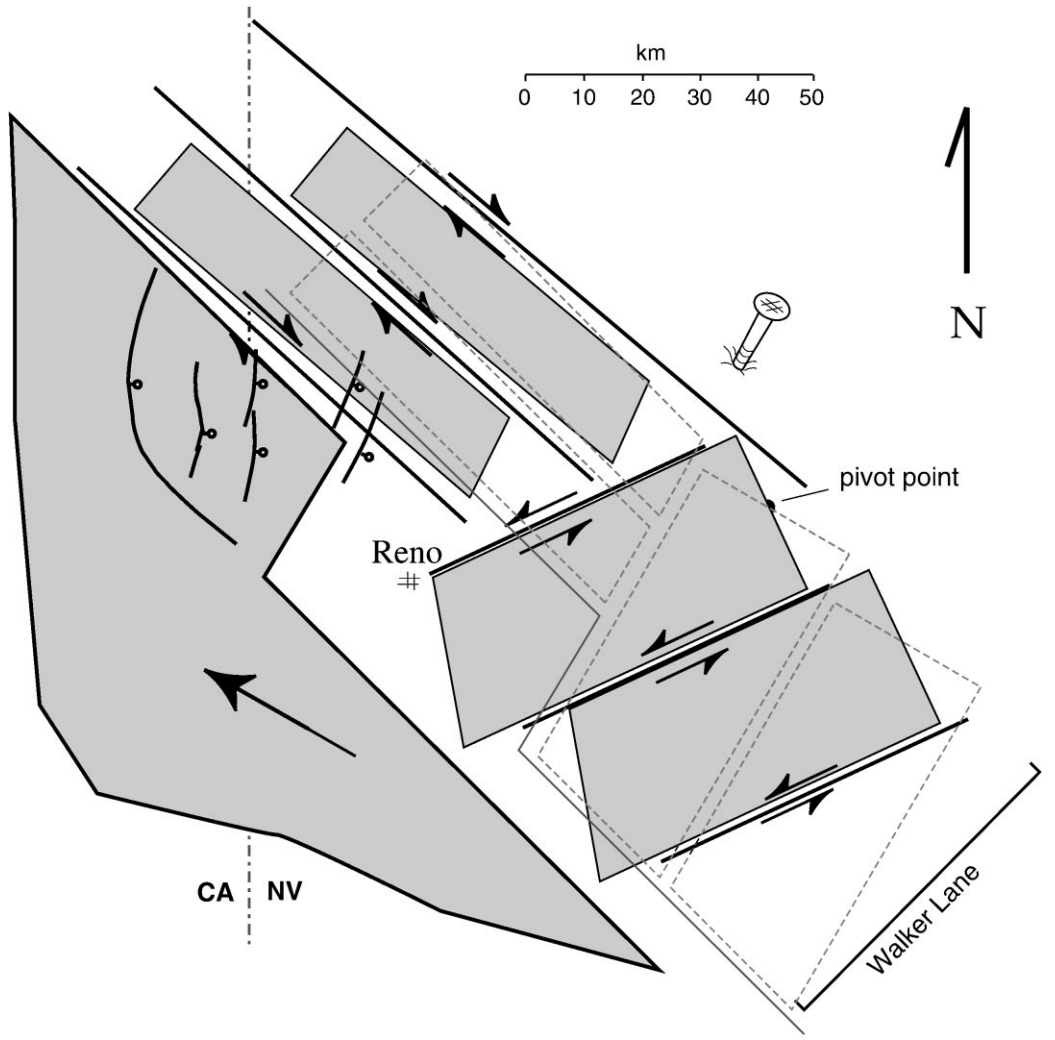


Fig. 10. Kinematic model of strain partitioning in the northern Walker Lane. Dashed lines shown initial positions of blocks. Dextral slip is accommodated by translation in the Pyramid Lake domain and by vertical-axis rotation in the Carson domain. See text for discussion.

blocks, where they impinge on the edge of the Sierra Nevada.

A testable prediction of this kinematic model is that slip on both sets of strike–slip faults (northwest-striking dextral faults and east-northeast-striking sinistral faults) can terminate abruptly, without the kinds of termination zones or transfer and accommodation zones normally required at the ends of major strike–slip faults. For example, if sinistral faults in the Carson domain exist only because they bound rotating blocks, a fault is not necessary beyond the end of the rotating block, and slip should terminate abruptly where vertical-axis rotation ceases. Similarly, features like the abrupt southern termination of the Warm Springs Valley fault mapped by Bonham (1969) are possible, with no decreased slip near the termination, if the fault exists only because it is the margin of a translating block.

Another prediction of the model is that gaps open up behind rotating or translating blocks; if these exist, they should be recognizable from topo-

graphic, geologic or geophysical evidence. Alternatively, the model could be constructed without gaps, creating significant and potentially recognizable overlaps where blocks impinge on adjacent blocks. Topographic and gravity lows along the eastern boundary of the Sierra correspond roughly to the gaps in the model between the Walker Lane and the Sierra. [These are, from north to south, the Reno area (Truckee Meadows), Washoe Valley and Carson Valley–Gardnerville.] Neogene sedimentary basins preserve a longer record of structural and topographic lows, along with paleogeographic information. There is a series of Neogene basins in northwestern Nevada and northeastern California, both within the Walker Lane and to the west of it, where extensional faulting is encroaching into the Sierra. Work in progress on the sedimentology, geochronology and structural history of these basins (e.g. Muntean et al., 1999; Trexler et al., 1999; Cashman et al., 1999) will elucidate both the paleogeography during deposition and the subsequent exhumation and deformation of each basin.

## 6. Discussion: implications for rate and timing of deformation in the northern Walker Lane

Our data provide new evidence for the timing of deformation in the northern Walker Lane. The clockwise rotations measured in the Nine Hill tuff of the Carson domain are comparable to those measured in the younger Pyramid sequence basalts of the Carson domain. This indicates that all of the rotation in the Carson domain has occurred since the eruption of the basalts (ca. 13–9 Ma) (Stewart et al., 1994). Although $21.8 \pm 0.7$ Ma mineralization occurs along northwest-striking sub-vertical faults in the Pyramid Lake domain (see Geologic Setting above), indicating that strike–slip faults existed at this time, the present deformation regime — in which strain is partitioned into domains of translation or rotation — seems to have been initiated much more recently.

Comparison of amount of rotation between rocks of different ages can, theoretically, determine the rate of rotation. It is not yet possible to do this with confidence in the Carson domain, however, because of the large margins for error on both the amounts of rotation and the ages of the rocks. The results from Churchill Butte are crudely consistent with a constant rotation rate (ca. $6 \pm 2^\circ$ Ma$^{-1}$), if rotation started soon after the eruption of the youngest Pyramid sequence rocks. (We measured $24.3 \pm 6.5^\circ$ rotation in 3.3–4.3 Ma rocks at Churchill Butte, compared to the $42.1 \pm 4.8^\circ$ to $54.3 \pm 3.9^\circ$ rotation recorded by 9–13 Ma rocks elsewhere in the domain.) An undated site near Vista which is mapped as 5–7 Ma Lousetown basalt (Bell and Bonham, 1987) has a $11.4 \pm 4.4^\circ$ CW rotation; if both correct and representative of the domain as a whole, this result suggests a decreasing rotation rate with time. New $^{40}Ar/^{39}Ar$ dating is in progress to improve our estimates of rotation rates.

Our new data on the timing and style of deformation contribute to a growing body of detailed information on the kinematics of deformation in the Walker Lane, and the changes in the deformation with time. Improved understanding of the structural evolution will ultimately allow us to differentiate between the tectonic influences on Walker Lane deformation. Several studies have documented multiple episodes of deformation since late Oligocene time, although the timing of these episodes differs somewhat between workers. In the central Walker Lane, Hardyman and Oldow (1991) infer different extension directions for three time periods: 29–18 Ma; 17–11 Ma; and 10 Ma–present. Dilles and Gans (1995) describe different styles of faulting in the time intervals 30–12 Ma, 11–8 Ma and 7 Ma–present in the northern Wassuk Range and Yerington. Several workers in the western Basin and Range have recognized a change to the current style of deformation in late Miocene time. Hardyman and Oldow (1991) describe the current deformation in the central Walker Lane as dextral displacement on northwest-striking sub-vertical faults, which commenced 10 Ma. Dilles and Gans (1995) interpret the most recent deformation in the Yerington area to be normal-oblique faulting accommodating NW–SE extension, starting 7 Ma. Minor (1995), working farther south, documented a change in extension direction from WSW to NW at ca. 9–11 Ma. Our new timing evidence for the initiation of partitioned strain in the northern Walker Lane (i.e. since the eruption of the 9–13 Ma basalts) is

consistent with the late Miocene change in deformation style noted by other workers. It both extends the evidence for a late Miocene change farther to the north, and suggests that this change was roughly synchronous throughout the entire latitude range in which it has been observed.

Several tectonic explanations have been proposed for the late Miocene change in deformation style in the Basin and Range; most agree that to some extent it is related to Pacific–North America plate boundary interactions. It has been attributed to the San Andreas transform starting to influence extension in the Basin and Range at ca. 10 Ma (e.g. Zoback et al., 1981). The plate circuit reconstruction of Atwater and Stock (1998) assumes that the continental margin has been attached to the Pacific plate (i.e. all strain is within the continent) since 18 Ma. They calculate a change in Pacific plate motion relative to stable North America (from N60°W to N37°W) at 8 Ma, and note that this change correlates closely to a change in direction of extension between the Colorado Plateau and the Sierra Nevada, i.e. that it is reflected in deformation within the continent. Studies analyzing *current* deformation within the continent — using techniques such as GPS surveying, VLBI/VLBA, and inversion of focal mechanisms — attempt to quantify individual components of the deformation, such as the translation and rotation of the Sierra Nevada microplate relative to the North American craton (e.g. Unruh et al., 1996; Hearn and Humphreys, 1998). Another approach is to examine the relative influence of gravitational potential energy and plate boundary interactions on the current intracontinental deformation (e.g. Unruh et al., 1998; Holt et al., 1998; Jones et al., 1999; Hearn and Humphreys, 1999). It is clear that the ultimate solution will incorporate both the current deformation and studies of Neogene and older rocks, which extend the kinematics back in time. Paleomagnetic studies add the unique measure of vertical-axis rotation to our understanding of the structural evolution.

## Acknowledgements

The authors are grateful to many colleagues for their contributions to this research; their participation has made it more enjoyable as well as more productive. Bob Karlin helped determine both magnetic mineralogy and demagnetization procedures, and provided unlimited access to the paleomagnetic laboratory at UNR. Mark Hudson, USGS, advised on many aspects of the paleomagnetic work and freely shared his knowledge and software with enthusiasm, patience and humor. Dick Hardyman was generous with his time, expertise and USGS truck, spending many field days mapping and sampling the Nine Hill tuff. Larry Garside, NBMG, spent time in the field with the authors on many occasions and shared his considerable knowledge of the geology of western Nevada. Many UNR geology students, both undergrads and grad students, cheerfully and capably assisted in field collection and laboratory analysis of paleomagnetic samples. Special thanks go to Jim Branch for his dedication, thoroughness and patience both in the field and in the lab. Jim Faulds, NBMG, Jim Trexler, UNR, and Mark Hudson, USGS, read early versions of the manuscript. Bernie Housen, Myrl Beck and Steve Gillett cheerfully provided advice and software on very short notice. Reviews by Elizabeth Shermer and John Stamatakos and comments by Editor Bernie Housen greatly improved the final paper. This research was funded by NSF Grants EAR91-05818, EAR94-05366 and a supplementary REU grant to Cashman and several colleagues. Fontaine's thesis work on the Pyramid Lake domain was also supported by two UNR Mackay School of Mines/USGS Fellowships.

## References

Albino, G., 1992. Washington Hill prospect. In: Craig, S. (Ed.), Geological Society of Nevada Spring Field Trip No 2 Guidebook: Geological Society of Nevada Special Publication 15.

Anderson, L.W., Hawkins, F.F., 1984. Recurrent Holocene strike–slip faulting, Pyramid Lake fault zone, western Nevada: Geology 12, 681–684.

Atwater, T., 1970. Implications of plate tectonics for the Cenozoic tectonic evolution of western North America: Geological Society of America Bulletin 81, 3513–3536.

Atwater, T., Stock, J., 1998. Pacific-North America plate tectonics of the Neogene southwestern United States — an update: International Geological Review 40, 375–402.

Bell, J.W., 1984. Quaternary fault map of Nevada, Reno sheet: Nevada Bureau of Mines and Geology Map 79, 1:250 000.

Bell, J.W., Bonham Jr, H.F., 1987. Geologic map of the Vista quadrangle, Nevada: Nevada Bureau of Mines and Geology Map 4Hg, 1:24 000.

Bonham, H.F., 1969. Geology and mineral deposits of Washoe and Storey counties, Nevada: Nevada Bureau of Mines and Geology Bulletin 70, 140 pp.

Bonham, H.F., Bell, J.W., 1993. Geology of the Steamboat quadrangle, Nevada: Nevada Bureau of Mines and Geology, MapFg, 1:24 000.

Cashman, P.H., Trexler, J.H., Jr., Henry, C.D., Perkins, M., 1999. Deformation recorded in the Neogene Verdi basin, Sierra Nevada — Basin and Range Transition, western Nevada (abs.), Geol. Soc. America Abstracts with Programs.

Castor, S.B., Garside, L.J., dePolo, C.M., 1999. Geologic map of the west half of the Moses Rock quadrangle, Nevada: Bureau of Mines and Geology Open-File Map 99-11, 1:24 000.

Cordy, G.E., 1985. Geologic map of the Reno NE quadrangle, Nevada: Nevada Bureau of Mines and Geology Map 4Cg, 1:24 000.

Deino, A.L., 1985. Stratigraphy, chemistry, K–Ar dating and paleomagnetism of the Nine Hill Tuff, California–Nevada, Part I, Miocene–Oligocene tuffs of Seven Lakes Mountain, California–Nevada, Part II: Ph.D. dissertation, Berkeley. p. 432.

Deino, A.L., 1989. Single-crystal 40Ar/39Ar dating as an aid in correlation of ash flows: examples from the Chimney Spring/New Pass tuffs and Nine Hill/Bates Mountain tuffs of California and Nevada (abs.): New Mexico Bureau of Mines and Mineral Resources Bulletin 131, 70.

Dilles, J.H., Gans, P.B., 1995. The chronology of Cenozoic volcanism and deformation in the Yerington area, western Basin and Range and Walker Lane: Geological Society of America Bulletin 107, 474–486.

Dokka, R.K., Travis, C.J., 1990. Role of the eastern California shear zone in accommodating Pacific–North America plate motion: Geophysical Research Letters 17 (9), 1323–1326.

Ekren, E.B., 1985a. Geologic map of the Gabbs Mountain, Mount Ferguson, Luning and Sunrise Flat quadrangles, Mineral and Nye counties, Nevada: U.S. Geological Survey map I-1577. U.S. Geological Survey, USA. 1:48 000.

Ekren, E.B., 1985b. Geologic map of the Win Wan Flat, Kincaid NW, Kincaid and Indian Head Peak quadrangles, Mineral County, Nevada: U.S. Geological Survey map I-1578. U.S. Geological Survey, USA. 1:48 000.

Ekren, E.B., 1986a. Geologic map of the Mount Annie NE, Mount Annie, Ramsey Spring and Mount Annie SE quadrangles, Mineral and Nye counties, Nevada: U.S. Geological Survey map I-1579. U.S. Geological Survey, USA. 1:48 000.

Ekren, E.B., 1986b. Geologic map of the Murphys Well, Pilot Cone, Copper Mountain and Poinsettia Spring quadrangles, Mineral county, Nevada: U.S. Geological Survey map I-1576. U.S. Geological Survey, USA. 1:48 000.

Ekren, E.B., Byers Jr, F.M., 1984. The Gabbs Valley Range — a well-exposed segment of the Walker Lane in west-central Nevada: In: Lintz Jr, J. (Ed.), Western Geologic Excursions vol. 4. Geological Society of America Guidebook Annual Meeting, Reno, NV, pp. 204–215.

Fisher, R., 1953. Dispersion on a sphere. Proceedings of the Royal Society of London 217, 295–305.

Fontaine, S.A., 1997. Structural and paleomagnetic analysis of the Pyramid Lake domain, northern Walker Lane, west-central Nevada. M.Sc. thesis, University of Nevada, Reno.

Garside, L.J., Bonham Jr, H.F., 1992. Olinghouse mining district, Washoe county, Nevada. In: Craig, S.D. (Ed.), Tectonics and Mineralization of the Walker Lane: Geological Society of Nevada Proceedings. Geological Society of Nevada, Nevada, pp. 227–238.

Garside, L.J., Niles, F.L., 1998. Geologic map of the Griffith Canyon quadrangle, Washoe County, Nevada: Nevada Bureau of Mines and Geology Open-File Map 99-4. Nevada Bureau of Mines and Geology, Nevada. 1:24 000.

Garside, L.J., Castor, S.B., dePolo, C.M., Davis, D.A., 1999. Geologic map of the Fraser Flat quadrangle, Nevada: Nevada Bureau of Mines and Geology Open-File Map 99-10. Nevada Bureau of Mines and Geology, Nevada. 1:24 000.

Greene, R.C., Stewart, J.H., John, D.A., Hardyman, R.F., Silberling, N.J., Sorensen, M.L., 1991. Geologic map of the Reno $1^\circ \times 2^\circ$ quadrangle, Nevada and California: USGS Map MF-2154-A. USGS, USA. 1:250 000.

Grose, T.L.T., 1993. The Walker Lane belt in northeastern California (abs.): Geological Society of America Abstracts with Programs 25, 44–45.

Grose, T.L.T., Wagner, D.L., Saucedo, G.J., Medrano, M.D., 1989. Geologic map of the Doyle 15-minute quadrangle, Lassen and Plumas counties, California: California Division of Mines and Geology Open-File Report 89-32. California Division of Mines and Geology, California. scale 1:62 500.

Hardyman, R.F., 1984. Strike–slip normal and detachment faults in the northern Gillis Range Walker Lane of west-central Nevada. In: Lintz, J.R. (Ed.), Western Geological Excursions. Geological Society of Nevada, Reno, pp. 184–199.

Hardyman, R.F., Oldow, J.S., 1991. Tertiary tectonic framework and Cenozoic history of the central Walker Lane, Nevada. In: Raines, G.L., Lisle, R.E., Schafer, R.W., Wilkinson, W.H. (Eds.), Geology and Ore Deposits of the Great Basin. Geological Society of Nevada, Reno, NV, pp. 279–301.

Hardyman, R.F., Ekren, E.B., Byers Jr, F.M., 1975. Cenozoic strike–slip, normal and detachment faults in the northern part of the Walker Lane, west-central Nevada (abs.): Geological Society of America Abstracts with Programs 7 (7), 1100.

Hearn, E.H., Humphreys, E.D., 1998. Kinematics of the southern Walker Lane belt and the motion of the Sierra Nevada block. Journal of Geophysical Research 103, B11, 27033–27049.

Hearn, E.H., Humphreys, E.D., 1999. Kinematics of the south-

ern Walker Lane belt and the motion of the Sierra Nevada block (abs.): EOS, Transactions, AGU 80, F207.

Henrichs, D.F., 1967. Paleomagnetism of the Plio-Pleistocene Lousetown formation, Virginia City, Nevada. Journal of Geophysic Research 72 (12), 3277–3293.

Holt, W.E., Flesch, L.M., Shen-Tu, B., Haines, A.J., 1998. The kinematics and dynamics of the western U.S. from Quaternay fault data, GPS and VLBI velocities and topography and geoid data (abs.): EOS, Transactions, AGU 79 (45), F206.

John, D.A., Garside, L.J., Wallace, A.R., 1999. Magmatic and tectonic setting of Late Cenozoic epithermal gold-silver deposits in northern Nevada with an emphasis on the Pah Rah and Virginia Ranges and the northern Nevada Rift. In: Kizis, J.A. (Ed.), Low-Sulfidation Gold Deposits in Northern Nevada, Geological Society of Nevada Special Publication 29, 64–158.

Jones, C.H., Sonder, L.J., Unruh, J.R., 1999. Body forces in western U.S. deformation: engine, steering or radio? (abs.): EOS, Transactions, AGU 80, F207.

Kirschvink, J.L., 1980. The least-square line and plane and the analysis of paleomagnetic data. Geophys. J. R. Astron. Soc. 62, 699–718.

Locke, A., Billingsley, P.R., Mayo, E.B., 1940. Sierra Nevada tectonic patterns. Geology Society of America Bulletin 51, 513–540.

Minor, S.A., 1995. Superposed local and regional paleostresses: fault-slip analysis of Neogene extensional faulting near coeval caldera complexes, Yucca Flat, Nevada. Journal of Geophysical Research 100, 10507–10528.

Moore, J.G., 1969. Geology and mineral deposits of Lyon, Douglas and Ormsby counties, Nevada: Nevada Bureau of Mines and Geology Bulletin 75, 45.

Muntean, T.W., Cashman, P.H., Trexler Jr, J.H., Henry, C.D., 1999. Tectonic evolution of the Gardnerville sedimentary basin, western Nevada (abs.): Geological Society of America Abstracts with Programs 31.

Nelson, M.R., Jones, C.H., 1987. Paleomagnetism and crustal rotations along a shear zone, Las Vegas Range, southern Nevada. Tectonics 6, 13–33.

Oldow, J.S., 1992. Late Cenozoic displacement partitioning in the northern Great Basin. In: Craig, S.D. (Ed.), Walker Lane Symposium Structure Tectonics and Mineralization of the Walker Lane. Geological Society of Nevada, Reno, NV.

Saucedo, G.J., Wagner, S.L., 1992. Geologic map of the Chico quadrangle. California Division of Mines and Geology, Regional Geologic Map Series Map No. 7A. California Division of Mines and Geology, California. scale 1:250 000.

Silberman, M.L., White, D.E., Keith, T.E.C., Dockter, R.D., 1979. Duration of hydrothermal activity at Steamboat Springs, Nevada, from ages of spatially associated volcanic rocks: US Geological Survey Professional Paper 458-D, 14 pp.

Speed, R.C., Cogbill, A.H., 1979. Candelaria and other left-oblique slip faults in the Candelaria region, Nevada: Geological Society of America Bulletin 90, 149–163.

Stewart, J.H., 1988. Tectonics of the Walker Lane belt western Great Basin — Mesozoic and cenozoic deformation in a zone of shear. In: Ernst, W.G. (Ed.), Metamorphism and Crustal Evolution of the Western United States. Englewood Cliffs, Prentice Hall, New Jersey, pp. 683–713.

Stewart, J.H., 1999. Geologic map of the Carson $30 \times 60$ min quadrangle, Nevada: Nevada Bureau of Mines and Geology Map 118, 1:100 000.

Stewart, J.H., McKee, E.H., John, D.A., 1994. Map showing compilation of isotopic ages of Cenozoic rocks in the Reno 1°x2° quadrangle, Nevada and California: USGS map MF-2154-D, 1:250 000.

Trexler Jr, J.H., Cashman, P.H., Henry, C.D., 1999. A syntectonic Neogene basin in western Nevada (abs.): Geological Society of America Abstracts with Programs 31.

Unruh, J.R., Twiss, R.J., Hauksson, E., 1996. Seismogenic deformation field in the Mojave block and implications for the tectonics of the Eastern California Shear Zone. Journal of Geophysical Research 101, 8335–8361.

Unruh, J.R., Hauksson, E., Montastero, F.C., Hasting, M., 1998. Seismogenic deformation in the Coso Range, east-central California: NW dextral shear along the eastern margin of the Sierra Nevada microplate (abs.): EOS, Transactions, AGU 79 (45), F564–F565.

Vandamme, D., 1994. A new method to determine paleosecular variation. Physics of the Earth and Planetary Interiors 85, 131–142.

Vikre, P.G., McKee, E.H., Silberman, M.L., 1988. Chronology of Miocene hydrothermal and igneous events in the western Virginia Range, Washoe, Storey and Lyon counties, Nevada: Economic Geology 83, 864–874.

Wills, C.J., Borchardt, G., 1993. Holocene slip rate and earthquake recurrence on the Honey Lake fault zone, northeastern California: Geology 21, 853–856.

Zoback, M.L., Anderson, R.E., Thompson, G.A., 1981. Cainozoic evolution of the state of stress and style of tectonism in the Basin and Range province of the western United States. Royal Society of London Philosophical Transactions A300, 407–434.